JACS
JOURNAL OF THE AMERICAN CHEMICAL SOCIETY
Article
pubs.acs.org/JACS

Potentiometric, Electronic, and Transient Absorptive Spectroscopic Properties of Oxidized Single-Walled Carbon Nanotubes Helically Wrapped by Ionic, Semiconducting Polymers in Aqueous and Organic Media

Pravas Deria, Jean-Hubert Olivier, Jaehong Park, and Michael J. Therien*

Department of Chemistry, French Family Science Center, Duke University, 124 Science Drive, Durham, North Carolina 27708-0346, United States

Supporting Information

ABSTRACT: We report the first direct cyclic voltammetric determination of the valence and conduction band energy levels for noncovalently modified (6,5) chirality enriched SWNTs [(6,5) SWNTs] in which an aryleneethynylene polymer monolayer helically wraps the nanotube surface at periodic and constant morphology. Potentiometric properties as well as the steady-state and transient absorption spectroscopic signatures of oxidized (6,5) SWNTs were probed as a function of the electronic structure of the aryleneethynylene polymer that helically wraps the nanotube surface, the solvent dielectric, and nanotube hole polaron concentration. These data: (i) highlight the utility of these polymer-SWNT superstructures in experiments that establish the potentiometric valence and conduction band energy levels of semiconducting carbon nanotubes; (ii) provide a direct measure of the (6,5) SWNT hole polaron delocalization length (2.75 nm); (iii) determine steady-state and transient electronic absorptive spectroscopic signatures that are uniquely associated with the (6,5) SWNT hole polaron state; and (iv) demonstrate that modulation of semiconducting polymer frontier orbital energy levels can drive spectral shifts of SWNT hole polaron transitions as well as regulate SWNT valence and conduction band energies.

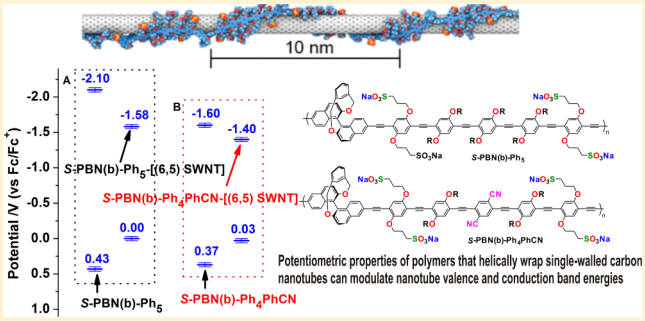

INTRODUCTION

Single-walled carbon nanotubes (SWNTs) possess unique optical[1] and electronic properties,[2] which combined with their unidirectional charge carrier pathway[3] have defined attractive nanoscale materials for photovoltaic,[4] field-effect transistor,[5] light-emitting diode,[6] and sensor[7] devices. Optoelectronic devices that exploit SWNTs require fundamental understanding of nanotube potentiometric properties.[8] Spectroelectrochemical methods, that have been used to evaluate SWNT redox potentials,[8a,9] monitor typically the bleaching of SWNT excitonic transitions as a function of electrode potential or the concentration of an added redox reagent; these experiments have often lacked straightforward interpretation, as such studies have been generally carried out on SWNT samples featuring heterogeneous distributions of nanotube chiralities and lengths that give rise to a vis-NIR spectral window characterized by a plethora of overlapping electronic transitions. Inconsistent use of internal potentiometric standards makes comparisons of various spectroelectrochemically determined SWNT valence and conduction band energy levels difficult.[8a,b,9] Furthermore, commonly used dispersing agents (surfactants) that provide individualized SWNTs in solution reduce medium dielectric strength and diminish heterogeneous electron transfer kinetics through insulation of the nanotube surface; diminishing the typically high surfactant:SWNT molar ratios used in these experiments, however, drives formation of SWNT bundles and films and calls into question what is actually being measured under such experimental conditions.[10]

We report the first direct cyclic voltammetric determination of redox potentials for noncovalently modified semiconducting SWNTs. These experiments exploit conjugated, highly charged aryleneethynylene polymers that exfoliate, individualize, and disperse SWNTs via a single-chain helical wrapping mechanism.[11,12] Such polymers (Chart 1) provide robust, helical superstructures wherein the polymer remains adhered to the SWNT surface; structural studies establish self-assembled superstructures in which the semiconducting polymer wraps the nanotube at periodic and constant morphology in a variety of aqueous and organic solvents.[11,12,12f]

Polymers ***S*-PBN(b)-Ph$_5$**, ***S*-PBN(b)-Ph$_4$PhCN**, and ***S*-PBN-(b)-Ph$_2$PZn$_2$** (Chart 1) have previously been established to wrap SWNTs in an exclusive left-handed fashion; the corresponding polymer-SWNT superstructures have been

Received: July 28, 2014
Published: September 11, 2014

dx.doi.org/10.1021/ja507457z | J. Am. Chem. Soc. 2014, 136, 14193−14199

Chart 1. Molecular Structures of *S*-PBN(b)-Ph_5, *S*-PBN(b)-Ph_4PhCN, and *S*-PBN(b)-Ph_2PZn_2 Polymers, Along with a Schematic Representation[11] of an [Arylene]ethynylene Polymer-Wrapped SWNT Superstructure Derived from Atomistic Molecular Dynamics Simulations

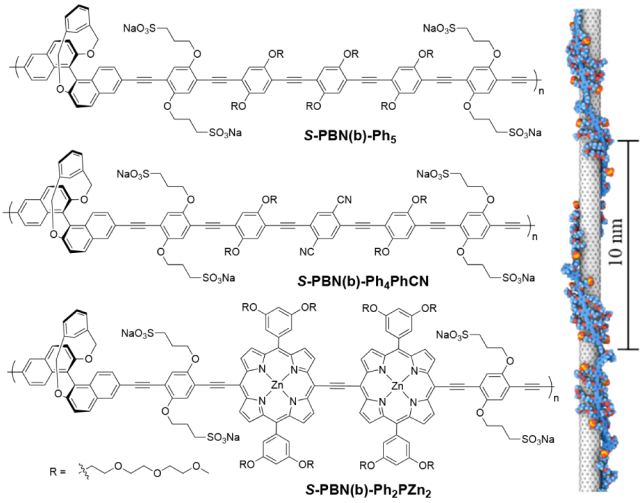

structurally characterized.[11,12g] The potentiometric and electronic structural studies reported herein investigate self-assembled nanostructures based on these Chart 1 polymers and (6,5) chirality enriched SWNTs, obtained in >85% purity through a combination of linear and nonlinear density gradient ultracentrifugation;[11,12c,h,13] cyclic voltammetric measurements probe high-density drop-cast films of these polymer-SWNT superstructures on glassy carbon electrodes. Note that single-chain SWNT helical wrapping by these highly charged semiconducting polymers circumvents bundle formation, maintaining individualized SWNTs at a minimal surfactant (polymer):SWNT mass ratio.[10b,11,12,12g] These studies that examine SWNT potentiometric properties and chronicle ground- and excited-state electronic transitions at various SWNT hole polaron densities: (i) establish methods that directly determine SWNT valence and conduction band energy levels and (ii) demonstrate that SWNT potentiometric and excitonic properties can be modulated by the nature of the electronic structure of the semiconducting polymer that wraps its surface.

EXPERIMENTAL SECTION

Materials. ***S*-PBN(b)-Ph_5, *S*-PBN(b)-Ph_4PhCN**, and ***S*-PBN(b)-Ph_2PZn_2** (Chart 1) polymers were synthesized and characterized as previously described.[11] CoMoCat SWNTs were obtained from Sigma-Aldrich as a freeze-dried powder and used as starting material for density gradient (DG) purification to obtain samples enriched with (6,5) chirality tubes. Detailed synthetic and experimental procedures are provided in the Supporting Information. Air-sensitive solids were handled in a Braun 150-M glovebox. Standard Schlenk techniques were employed to manipulate air-sensitive solutions. Tris(4-bromophenyl)-ammoniumyl hexachloroantimonate and K_2IrCl_6 were purchased from Aldrich, manipulated under inert atmosphere, dissolved in appropriate solvents, and stored in sealed Schlenk tubes under argon. SmI_2 (1 M in THF) was purchased from Aldrich and diluted accordingly under argon atmosphere. The M_n values of the aryleneethynylene polymers ***S*-PBN(b)-Ph_5, *S*-PBN(b)-Ph_4PhCN**, and ***S*-PBN(b)-Ph_2PZn_2** (Chart 1) were respectively determined to be ~20.78, 14.5, and 20.1 kDa by gel permeation chromatography (GPC); polymers ***S*-PBN(b)-Ph_5, *S*-PBN(b)-Ph_4PhCN**, and ***S*-PBN(b)-Ph_2PZn_2** possess correspondingly ~46, 38, and 28 respective arylene units (where each binaphthalene component is counted as a single arylene unit).[11]

Instrumentation. Electronic absorption spectra were recorded on a Varian 5000 UV−vis−NIR spectrophotometry system. IR spectra were recorded on a Bruker Tensor 27 in ATR mode. Cyclic voltammetric measurements were performed using a Bioanalytical Systems (BASi) Epsilon potentiostat and a single-compartment electrochemical cell. Emission spectra were recorded on an Edinburgh FLSP920 steady-state luminescence instrument that utilizes a Xe lamp as an excitation source and a Hamamatsu H10330-75 (900−1700 nm) PMT detector. Emission spectra were recorded over a 950−1400 nm spectral range (1 nm steps; integration time = 0.1 s) by exciting the E_{22} transition (~580 nm) of the [(6,5) SWNT] samples. Ground-state Raman spectra were recorded using a custom Raman spectrometry system that features a Princeton Instrument Acton SP2360i 300 mm spectrograph (Roper Scientific, Trenton, NJ, USA) outfitted with multi gratings to cover a 250−1100 nm spectral regime. Light detection through the spectrograph is provided via a Princeton Instrument Acton PIXIS 400 BR CCD detector (250−1100 nm, 1300 × 400 pixels, 20 um pixel size, back-illuminated deep-depletion for enhanced sensitivity throughout the NIR; Roper Scientific, Trenton, NJ, USA). A 532 nm diode-pumped solid-state laser (100 mW; Cobolt Samba 100, Cobolt AB Lasers, Solna, Sweden) was used as a light source; the excitation power was 13 mW. All spectroscopic measurements were carried out at 20 ± 1 °C. Ultrafast transient absorption (TA) spectra were obtained using standard pump−probe methods described previously.[12h] Following all pump−probe TA experiments, electronic absorption spectra verified that the carbon nanotube and polymer−nanotube superstructure samples were robust.

Computational Methods. Electronic absorption spectra of 4 and 8 nm long [(6,5) SWNT] segments, having respective oxidation states of +2 and +4, were calculated using time-dependent density functional theory (TD-DFT//B3LYP/6-31G; Gaussian-09 software package).[14] Terminal C atoms of the SWNT segments were "capped" with H atoms, and the structures were optimized using AM1 basis functions. Electronic transitions were obtained via TD-DFT calculations of 15−24 excited states for these AM1-optimized structures using the B3LYP/6-31G basis set.[15] Further details are provided in the Supporting Information.

Sample Preparation. Polymer-wrapped [(6,5) SWNT] samples were prepared and purified following procedures described earlier.[11] For the cyclic voltammetric experiments, an aqueous solution (2 mL, ~1 mg/mL) of the polymer-wrapped [(6,5) SWNTs] sample was reacted with 50 μL 15-C-5 crown ether, after which the solvent was removed under vacuum. The resulting sticky green solid was redissolved in 1 mL of MeOH, drop casted (5 μL × 3) on the glassy carbon electrode, evaporated under a stream of N_2 gas, and then dried under vacuum. Likewise, samples for redox reagent titration experiments were prepared as follows: to an aqueous solution (4 mL, ~1 mg/mL) of ***S*-PBN(b)-Ph_5-[(6,5) SWNTs]**, 50 μL of 15-C-5 crown ether was added, after which the solvent was removed under vacuum. The resulting solid was mixed with 20 mg of the bulky amphiphilic counterion (Chart S1) in a 1:1 DMSO:MeOH solvent mixture at 60 °C. The resulting precipitate was filtered and washed (7:3 THF:MeOH; 30 mL) through a 0.20 μm hydrophobic PTFE membrane (Millipore-FGLP) to remove the excess of free counter-cation.

Cyclic Voltammetric Studies of Polymer and Polymer-Wrapped (6,5) SWNT Samples. Electrochemical measurements were carried out using a literature procedure widely adopted for electrochemical characterization of conjugated semiconducting polymers.[16] Cyclic voltammetric data were recorded using a single-compartment electrochemical cell and a standard three-electrode configuration that utilized a glassy carbon working electrode, a platinum wire counter electrode, and a Ag/AgCl (3 M KCl) reference electrode. The reference electrode was separated from the bulk solution by a junction bridge filled with the corresponding solvent/electrolyte solution. The ferrocene/ferrocenium redox couple was utilized as an internal potentiometric standard. Electrochemical measurements utilized tetra-*n*-butylammonium hexafluorophosphate

dx.doi.org/10.1021/ja507457z | J. Am. Chem. Soc. 2014, 136, 14193−14199

(0.1 M) as the electrolyte in anhydrous CH_2Cl_2 solvent under argon. For each polymer and corresponding polymer-wrapped [(6,5) SWNT] sample, cathodic and anodic half cycles (50 mV/s) were scanned separately. Further detail concerning these experiments is provided in the Supporting Information.[16]

RESULTS AND DISCUSSION

Figure 1 describes the potentiometrically determined HOMO and LUMO energy levels of ***S*-PBN(b)-Ph$_5$**, ***S*-PBN(b)-Ph$_4$PhCN**, ***S*-PBN(b)-Ph$_2$PZn$_2$** polymers, along with the valence and conduction band energies of their corresponding polymer-[(6,5) SWNT] superstructures (Supporting Information, section SI-5). Oxidation potentials measured for ***S*-PBN(b)-Ph$_5$-[(6,5) SWNT]** and ***S*-PBN(b)-Ph$_4$PhCN-[(6,5) SWNT]** samples were essentially identical (~0.0 V); note that the SWNT valence band energy levels of these polymer-SWNT superstructures reside at significantly lower potential than that of the potentiometrically determined HOMO energy levels of their respective, corresponding polymers. The potentiometrically determined HOMO–LUMO energy gaps for these ***S*-PBN(b)-Ph$_5$-[(6,5) SWNT]**, ***S*-PBN(b)-Ph$_4$PhCN-[(6,5) SWNT]**, and ***S*-PBN(b)-Ph$_2$PZn$_2$-[(6,5) SWNT]** constructs (Figure 1) track with the magnitudes of their respective $E_{00} \rightarrow E_{11}$ transition energies, which are diminished with respect to that determined for classic, surfactant-dispersed (6,5) SWNT samples (Figure S1).[11] Reacting ***S*-PBN(b)-Ph$_5$-[(6,5) SWNT]** and ***S*-PBN(b)-Ph$_4$PhCN-[(6,5) SWNT]** samples with K_2IrCl_6 (+0.87 V vs NHE in H_2O; ~0.65 V vs SCE; ~0.2 V vs Fc/Fc$^+$)[17] causes bleaching of the $E_{00} \rightarrow E_{11}$ transition at 1000 nm (Figures 2A, B) indicating oxidation of the underlying [(6,5) SWNTs];[8b,18] note that in these experiments, the polymer that helically wraps the SWNT surface remains unoxidized, as no significant bleaching of the $\pi-\pi^*$ transitions at ~400 nm can be detected (Figure 2A-B). While a potentiometrically determined conduction band energy level of −1.58 V (vs Fc/Fc$^+$) was ascertained for ***S*-PBN(b)-Ph$_5$-[(6,5) SWNTs]** (Figure 1), note that the corresponding potential for ***S*-PBN(b)-Ph$_4$PhCN-[(6,5) SWNTs]** is stabilized by 180 mV: this perturbation to the SWNT conduction band energy level is attributed to the electronic structural impact of the ***S*-PBN(b)-Ph$_4$PhCN** polymer that wraps the nanotube surface.

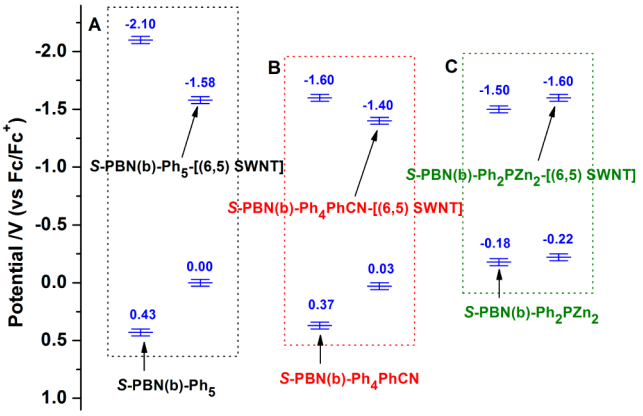

Figure 1. Potentiometrically determined HOMO and LUMO energy levels (relative to the Fc/Fc$^+$ redox couple, used as an internal standard) of the ***S*-PBN(b)-Ph$_5$**, ***S*-PBN(b)-Ph$_4$PhCN**, ***S*-PBN(b)-Ph$_2$PZn$_2$** polymers, along with the valence and conduction band energies of their corresponding polymer-[(6,5) SWNT] superstructures. Experimental conditions: CH_2Cl_2 solvent, 0.1 M $TBAPF_6$, 50 mV/s scan rate, glassy carbon working electrode, Ag/AgCl reference electrode.

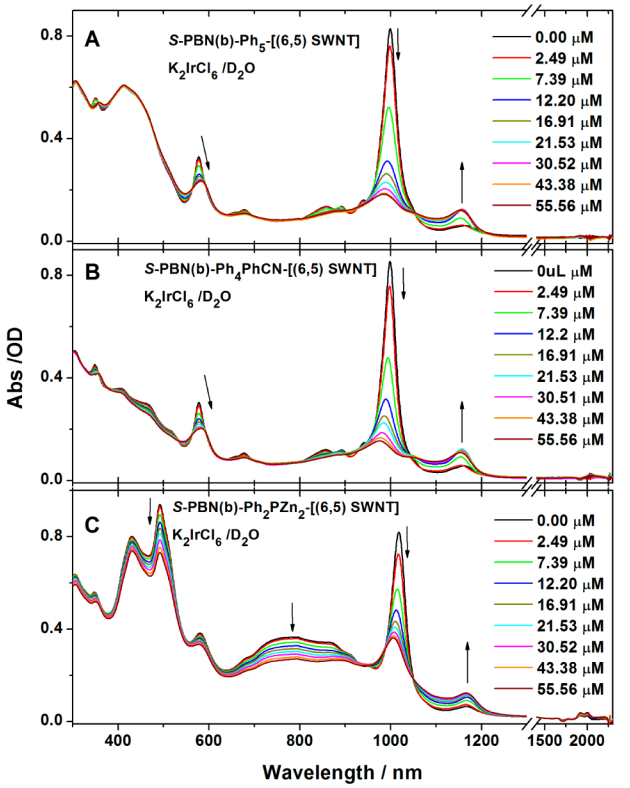

Figure 2. UV–vis–NIR steady-state absorption spectra that chronicle the oxidative titration of: (A) ***S*-PBN(b)-Ph$_5$-[(6,5) SWNTs]**, (B) ***S*-PBN(b)-Ph$_4$PhCN-[(6,5) SWNTs]**, and (C) ***S*-PBN(b)-Ph$_2$PZn$_2$-[(6,5) SWNTs]** with K_2IrCl_6 (aqueous solvent). Panel A–C insets correlate the observed electronic absorption spectrum with the oxidant concentration present. Experimental conditions: [(6,5) SWNT] ~72.3 nM; SWNT length = 700 ± 50 nm; argon atmosphere; T = 25 °C; optical path length = 2 mm.

Previous work establishes that metathesis reactions that replace the sulfonate counterion (sodium) of these polymer-SWNT superstructures (Chart 1) with appropriate bulky amphiphilic counterions provide corresponding organic solvent soluble polymer–nanotube hybrids (Supporting Information).[12g] Redox titration experiments in which ***S*-PBN(b)-Ph$_4$PhCN-[(6,5) SWNTs]** were reacted with samarium iodide (−1.45 V vs Fc/Fc$^+$)[19] in THF solvent also evinced bleaching of the SWNT $E_{00} \rightarrow E_{11}$ transition, with no reduction evident of the ***S*-PBN(b)-Ph$_4$PhCN** polymer that wraps the nanotube surface (Supporting Information, section SI-8). Similar experiments carried out with ***S*-PBN(b)-Ph$_2$PZn$_2$-[(6,5) SWNTs]** (Figure 1; Supporting Information) demonstrate that polymers that helically wrap the SWNT surface can also be designed that destabilize the nanotube valence band energy level. Related data obtained for other examples of polymer–nanotube hybrid structures suggest that the SWNT exciton binding energy (E_{11}^b)[12b,20] can be impacted by the polymer-SWNT interaction. Congruent with these results, these experiments demonstrate a E_{11}^b value of 0.19 eV for ***S*-PBN(b)-Ph$_4$PhCN-[(6,5) SWNTs]**, 0.24 eV lower in energy than the benchmark value for 0.43 eV surfactant-dispersed **[(6,5) SWNTs]**.[20]

To further elucidate the optoelectronic properties of oxidized [(6,5) SWNTs] in these ***S*-PBN(b)-Ph$_5$-[(6,5) SWNT]**, ***S*-PBN(b)-Ph$_4$PhCN-[(6,5) SWNT]**, and ***S*-PBN(b)-Ph$_2$PZn$_2$-**

dx.doi.org/10.1021/ja507457z | J. Am. Chem. Soc. 2014, 136, 14193–14199

[(6,5) SWNT] superstructures, oxidative titration experiments were carried out in both aqueous and nonaqueous solvent and monitored over the UV−vis−NIR (300−2300 nm) spectral regime (Figures 2 and S8B); corresponding NIR emission and Raman spectral data can be found in the Supporting Information (Figures S6, S7, S10). Figure 2 electronic absorption data that chronicle the oxidative titration of ***S*-PBN(b)-Ph$_5$-[(6,5) SWNT]**, ***S*-PBN(b)-Ph$_4$PhCN-[(6,5) SWNT]**, and ***S*-PBN(b)-Ph$_2$PZn$_2$-[(6,5) SWNT]** superstructures highlight: (i) a progressive diminution of both the $E_{00} \rightarrow E_{11}$[8b,18,21] and $E_{00} \rightarrow E_{22}$[8b,18,21c] transition oscillator strength with increasing oxidant concentration; (ii) that a plateau oscillator strength value for these transitions is reached at an identical oxidant concentration (~17 μM for a 72.3 nM concentration of 700 nm-long (6,5) SWNTs; shown with an arrow in Figure 3A); (iii) spectral blue shifts of the $E_{00} \rightarrow E_{11}$[21]

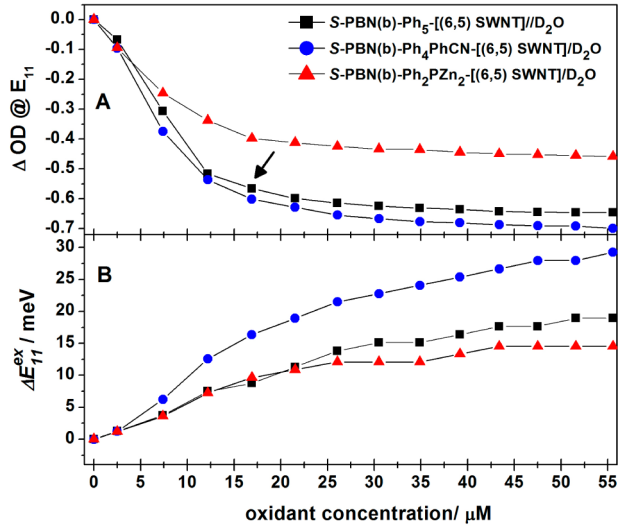

Figure 3. Oxidative titration data highlighting: (A) the progressive diminution of the $E_{00} \rightarrow E_{11}$ transition oscillator strength and (B) the magnitude of the $E_{00} \rightarrow E_{11}$ spectral blue shift observed with increasing oxidant concentration (Figure 2) for these polymer-[(6,5) SWNT] superstructures. The arrow in Panel A indicates that beyond this point of the titration, ΔOD is minimal. Experimental conditions: [(6,5) SWNT] ~72.3 nM; SWNT length = 700 ± 50 nm; argon atmosphere; T = 25 °C.

transition energy that range from ~12−32 cm^{-1} (Figure 3B) over the course of these oxidative titrations, and (iv) the rise of a new low energy transition at ~1150 nm[8b,21a,b] the oscillator strength of which tracks with increasing oxidant concentration.

Data summarized in Figure 3 indicate that both ***S*-PBN(b)-Ph$_5$-[(6,5) SWNT]** and ***S*-PBN(b)-Ph$_4$PhCN-[(6,5) SWNT]** samples in aqueous media show ~72% and ~32% bleaching of their respective initial $E_{00} \rightarrow E_{11}$ and $E_{00} \rightarrow E_{22}$ oscillator strengths at an oxidant concentration of ~17 μM (K_2IrCl_6); related theoretical work by Spataru and Léonard predicts that at a doping level of 0.6 h/nm, the $E_{00} \rightarrow E_{11}$ and $E_{00} \rightarrow E_{22}$ transition oscillator strengths should feature respective 83% and 30% reductions relative to that for a neutral SWNT.[21c] Note that an oxidant concentration of ~17 μM corresponds to ~1 hole per 2.75 nm [(6,5) SWNT] (or ~0.36 h/nm): at this oxidation level, each possible excitonic site of a neutral SWNT (~2.0 ± 0.7 nm in dimension)[20b,22] is doped with one hole, and further increases in oxidant concentration do not significantly effect in the $E_{00} \rightarrow E_{11}$ and $E_{00} \rightarrow E_{22}$ excitonic transition oscillator strengths. While earlier work[18,23] and the data summarized in Figures 2 and 3 (see also Supporting Information) emphasize that the experimentally accessible hole density in an oxidized semiconducting SWNT depends on the redox potential of the oxidant, the oxidant concentration, and the energy of the SWNT valence band (i.e., SWNT chirality), these results indicate that the SWNT hole polaron delocalization length (2.75 nm) is similar to that for the neutral SWNT exciton.[20b,24]

For these ***S*-PBN(b)-Ph$_5$-[(6,5) SWNT]**, ***S*-PBN(b)-Ph$_4$PhCN-[(6,5) SWNT]**, and ***S*-PBN(b)-Ph$_2$PZn$_2$-[(6,5) SWNT]** superstructures, the $E_{00} \rightarrow E_{11}$ transition energy manifests a blue shift upon oxidation. Theoretical work by Spataru and Léonard predicts that while oxidation of a semiconducting SWNT increases the $E_{00} \rightarrow E_{11}$ transition energy, significant reductions in the potentiometric band gap (E_{ii}^g) and exciton binding energy (E_{ii}^b) result from conduction band stabilization (Figure 4);[21c] the extent of these transition

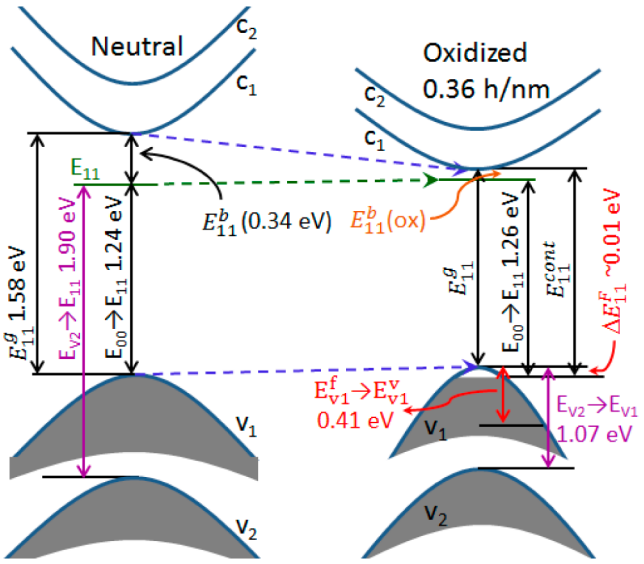

Figure 4. Energy diagrams illustrating the potentiometric band gap (E_{ii}^g) and exciton binding energy (E_{ii}^b) for the ***S*-PBN(b)-Ph$_5$-[(6,5) SWNT]** superstructure for neutral (left) and oxidized (right, ~0.36 h/nm) states; numerical values noted are determined from experimental data. The occupied valence electronic states are represented with gray-shaded areas, and the excitonic states are denoted with green lines. The highest occupied energy level of the oxidized SWNT was aligned with that of the neutral structure.[21c] Cross polarized $E_{V2} \rightarrow E_{11}$ and $E_{V2} \rightarrow E_{V1}$ transitions are shown in purple arrows,[28] and the intraband transitions (within the depleted v_1) are highlighted in red arrows.

and band energy perturbations tracks with the changes in the magnitude of dielectric screening that derives from nanotube hole doping. Using a classical band diagram picture,[25] Figure 4 highlights how E_{11}^g and E_{11}^b are impacted[21c] for a ***S*-PBN(b)-Ph$_5$-[(6,5) SWNT]** superstructure oxidized to achieve a hole density of ~0.36 h/nm. A hole-doped, depleted v_1 (Figure 4) is expected[21c] to increase the $E_{00} \rightarrow E_{11}$ transition energy; the corresponding Fermi level transition (ΔE_{11}^F; Figure 4) that appears in the far-IR at ≤100 cm^{-1} has previously been identified in free carrier doped SWNTs (see Supporting Information, sections SI-9 and 10).[26] The magnitude of the Fermi level transition energy (≤10 meV) matches the ~9−16 meV blue shift observed for the $E_{00} \rightarrow E_{11}$ transition due to v_1 band depletion upon oxidation of ***S*-PBN(b)-Ph$_5$-[(6,5)**

dx.doi.org/10.1021/ja507457z | J. Am. Chem. Soc. 2014, 136, 14193−14199

SWNT] and ***S*-PBN(b)-Ph$_4$PhCN-[(6,5) SWNT]** samples (Figure 2B); in this regard it is interesting to note that the predicted increase in the $E_{00} \rightarrow E_{11}$ transition energy for a semiconducting SWNT oxidized to a hole density of 0.6 h/nm is ~0.1 eV).[21c] Data summarized in Figures 2, 3B, and S9B suggest that the magnitude of this $E_{00} \rightarrow E_{11}$ blue shift (i.e., the observed increase in $E_{00} \rightarrow E_{11}$ transition energy that occurs with hole doping) can be impacted by both the electronic structure of the charged, semiconducting polymer[27] that wraps the SWNT surface and the solvent dielectric: such findings have heretofore lacked precedent. In contrast, due to large Franck–Condon overlap, exciton relaxation via NIR emission populates the highest-lying v_1 electronic states. Consistent with this expectation, NIR emission spectroscopic data (Figures S6 and 10) that probe ***S*-PBN(b)-Ph$_5$-[(6,5) SWNT]** samples in aqueous and CH_2Cl_2 solvents as a function of oxidant concentration demonstrate that the $E_{11} \rightarrow E_{00}$ transition energy (~1.24 eV) remains invariant relative to that for the neutral (6,5) SWNT (Figure 4).

A prominent spectroscopic feature of oxidized SWNTs is the appearance of a new low-energy electronic absorption[8b,21a,b] approximately 155–168 meV to the red of the $E_{00} \rightarrow E_{11}$ transition. For aqueous ***S*-PBN(b)-Ph$_5$-[(6,5) SWNT]** and ***S*-PBN(b)-Ph$_4$PhCN-[(6,5) SWNT]** samples and ***S*-PBN(b)-Ph$_5$-[(6,5) SWNTs]** in CH_2Cl_2 solvent, this low-energy transition is centered at 1156 nm, 168.5 meV lower in energy than the $E_{00} \rightarrow E_{11}$ transition (999 nm) observed for the corresponding neutral SWNT superstructures. For ***S*-PBN(b)-Ph$_2$PZn$_2$-[(6,5) SWNTs]**, this transition characteristic of oxidized (6,5) SWNTs appears at 1167 nm, 155.6 meV lower in energy than the corresponding $E_{00} \rightarrow E_{11}$ transition observed for the neutral polymer-wrapped SWNT superstructure (1018 nm; Figure 2). For these ***S*-PBN(b)-Ph$_5$-[(6,5) SWNT]**, ***S*-PBN(b)-Ph$_4$PhCN-[(6,5) SWNT]**, and ***S*-PBN(b)-Ph$_2$PZn$_2$-[(6,5) SWNT]** samples, this electronic absorption characteristic of oxidized (6,5) SWNTs: (i) does not display a transition energy dependence upon oxidant concentration, indicating that single species gives rise to the observed absorption; (ii) features a maximum oscillator strength ~1/7 of that observed for the corresponding neutral [(6,5) SWNT] $E_{00} \rightarrow E_{11}$ transition; and (iii) shows no discernible transition energy dependence upon the solvent dielectric.

Pioneering work by Tretiak established that SWNT excitonic transitions can be simulated using the TD-DFT method.[15] Similar TD-DFT calculations carried out on a 4 nm-long bare $[(6,5)\ SWNT]^{2+}$ model segment predict transitions of low oscillator strength at 1066 and 1210 nm, 266 and 404 meV to the red of the $E_{00} \rightarrow E_{11}$ like transition; as a 4 nm long [(6,5) SWNT] is of insufficient length to drive formation of semiconducting bands, these computed transitions formally involve respective [H-11 → LUMO (93%), H-9 → LUMO (4%)], and [H-9 → LUMO (93%), H-11 → LUMO (4%)] excitations (see Supporting Information, section SI-9; Figure S13; note that in these computed transitions that the orbital referred to as the LUMO of the $[(6,5)\ SWNT]^{2+}$ model structure corresponds to the HOMO for the analogous 4 nm-long neutral $[(6,5)\ SWNT]^{0}$ model segment). Likewise, these TD-DFT calculations carried out for this hypothetical 4 nm-long bare $[(6,5)\ SWNT]^{2+}$ species also predict transitions at 1666 and 1759 nm, 685 and 724 meV red to the $E_{00} \rightarrow E_{11}$ like transition, involving respective [H-7 → LUMO (60%), H-5 → LUMO (36%)], and [H-7 → LUMO (38%), H-5 → LUMO (59%)] excitations. As SWNT segment length increases beyond this 4 nm-long model system for the [(6,5) SWNT] hole polaron state, TD-DFT computed electronic transition energies will diminish as the density of discrete molecular orbitals characteristic of this calculation increases[29] and eventually coalesces to form bands,[30] as highlighted in Figure 4. Based on these considerations and the computed spectral transitions for the 4 nm-long bare $[(6,5)\ SWNT]^{2+}$ model, a hypothetical (and computationally inaccessible) TD-DFT calculation for an infinitely long [(6,5) SWNT] would be expected to show the coalescence of the 1066 and 1210 nm transitions as well as the 1666 and 1759 nm transitions: these band–band absorptions correspond to the $E_{V_2} \rightarrow E_{V_1}$ and $E^{f}_{V_1} \rightarrow E^{V}_{V_1}$ (filled v_1-to-vacant v_1) transitions shown in Figure 4. Given the close correspondence between computed and observed electronic transitions, the experimental absorptions observed at ~1155 nm (Figure 2) and 3400 cm^{-1} (Figure S14) for the ***S*-PBN(b)-Ph$_5$-[(6,5) SWNT]** superstructure oxidized to achieve a hole density of ~0.36 h/nm are thus assigned respectively to these $E_{V_2} \rightarrow E_{V_1}$ and $E^{f}_{V_1} \rightarrow E^{V}_{V_1}$ transitions. Although this ~1155 nm transition has been associated previously with trion (bound hole-exciton) generation,[21a,b] the spectroscopic and dynamical data acquired as a function of solvent dielectric and nanotube hole polaron density chronicled herein, coupled with these computational studies, suggest that this transition is best described as $E_{V_2} \rightarrow E_{V_1}$.

Figure 5 displays representative TA spectral data obtained for oxidized (0.36 h/nm) and neutral ***S*-PBN(b)-Ph$_5$-[(6,5) SWNTs]** in aqueous solvent, following $E_{00} \rightarrow E_{22}$ excitation. Previous studies established the TA spectral signatures of neutral (6,5) SWNTs over the 900–1400 nm spectral domain;

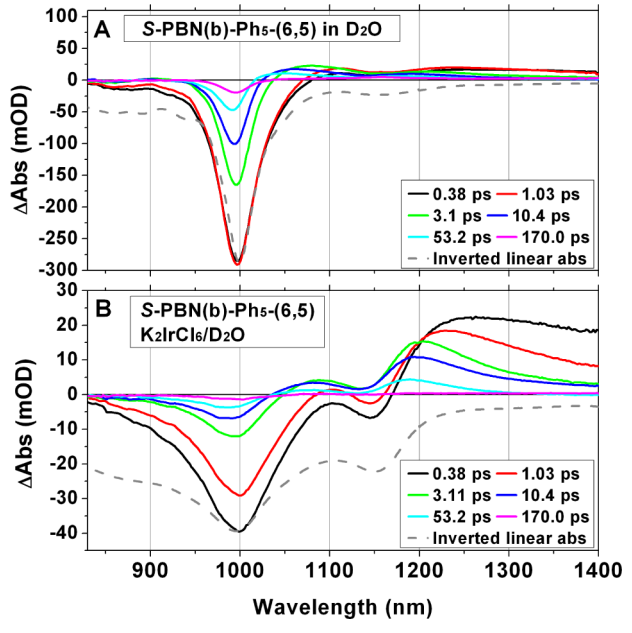

Figure 5. Representative TA spectra obtained for: (A) neutral ***S*-PBN(b)-Ph$_5$-[(6,5) SWNTs]** and (B) ***S*-PBN(b)-Ph$_5$-[(6,5) SWNTs]** oxidized to provide a hole polaron density of 0.36 h/nm, in aqueous solvent, at the time delays noted. Experimental conditions: (panels A, B) λ_{ex} = 580 nm; pulse energy = ~200–550 nJ/pulse; [(6,5) SWNT] = 84.6 nM; nanotube length = 700 ± 50 nm; T = 20 °C; magic angle polarization; (panel B) $[K_2IrCl_6]$ = 66.7 μM. Scaled steady-state absorption spectra (inverted dashed lines) are displayed for comparison.

dx.doi.org/10.1021/ja507457z | J. Am. Chem. Soc. 2014, 136, 14193–14199

these include a dominant $E_{00} \rightarrow E_{11}$ bleach (1000 nm) and three TA bands, observed to the red of this band at ~1100, ~1155, and 1200−1400 nm (Figure 5A).[12c,h] On the other hand, TA spectra obtained for oxidized ***S*-PBN(b)-Ph$_5$-[(6,5) SWNTs]** that feature a hole polaron density of 0.36 h/nm manifest ground-state bleaching (GSB) bands centered at both ~1000 and ~1150 nm as well as a TA signature having an absorption maximum near 1200 nm and a band shape that tails deeply into the NIR (Figure 5B); we note that earlier work has ascribed some of the long wavelength transient absorptive spectral features to $E_{00} \rightarrow E_{trion}$ transitions.[21a] A prominent feature of these GSB bands observed for oxidized (6,5) SWNTs is their spectral breadth. Note that the full-width-at-half-maximum (fwhm) determined at $t_{delay} \sim 1$ ps for the intense bleaching band manifold centered at 1000 nm (fwhm = 900 cm^{-1}) for oxidized ***S*-PBN(b)-Ph$_5$-[(6,5) SWNTs]**: the spectral breadth of this transition exceeds that determined for the analogous GSB band of neutral ***S*-PBN(b)-Ph$_5$-[(6,5) SWNTs]** by more than 500 cm^{-1} in aqueous solvent at an equivalent time delay. It is also noteworthy that the transient NIR spectral features characteristic of oxidized ***S*-PBN(b)-Ph$_5$-[(6,5) SWNTs]** (i.e., the GSB at 1000 nm and the TA band centered near 1200 nm) in aqueous solvent resemble closely the analogous signals observed for identical pump−probe experiments carried out in CH_2Cl_2 solvent (Figure S15); these TA spectral data, obtained over time delays ranging from 0.3 to 200 ps, thus indicate that the electronic transitions characteristic of oxidized ***S*-PBN(b)-Ph$_5$-[(6,5) SWNTs]** manifest little solvatochromism. With respect to the excited-state dynamics of oxidized (0.36 h/nm) ***S*-PBN(b)-Ph$_5$-[(6,5) SWNTs]**, these experiments demonstrate: (i) like that observed for neutral ***S*-PBN(b)-Ph$_5$-[(6,5) SWNTs]**, the time constant for $E_{22} \rightarrow E_{11}$ internal conversion occurs within the duration of the laser pulse (<100 fs)[24b,31] (Figure S16), and (ii) that the decay rate of the GSB signal intensity at 1000 nm is faster for oxidized (6,5) SWNTs with respect to that determined for neutral (6,5) SWNTs (Figures 5 and S16). Multiexponential fitting of the GSB recovery dynamics reveals that for neutral ***S*-PBN(b)-Ph$_5$-[(6,5) SWNTs]**: (time constant, τ (relative amplitude) $\tau_1 = 1.5$ ps (0.55), $\tau_2 = 11.1$ ps (0.25), $\tau_3 = 59.4$ ps (0.15), and $\tau_4 > 3$ ns (0.05); in contrast, for oxidized (0.36 h/nm) ***S*-PBN(b)-Ph$_5$-[(6,5) SWNTs]**, $\tau_1 = 0.8$ ps (0.69), $\tau_2 = 5.5$ ps (0.17), and $\tau_3 = 55.8$ ps (0.14). Note that only neutral (6,5) SWNTs evince ns time scale GSB recovery dynamics. These results are consistent with the existence of SWNT hole polaron states that are both delocalized and mobile[31] and congruent with the fact that even modest SWNT hole dopant can drive complete emission quenching (Figure S6).[31,32]

CONCLUSION

In summary, we have utilized three electronically distinct semiconducting polymers, previously established to wrap SWNTs in an exclusive left-handed helical fashion to provide ***S*-PBN(b)-Ph$_5$-[(6,5) SWNT]**, ***S*-PBN(b)-Ph$_4$PhCN-[(6,5) SWNT]**, and ***S*-PBN(b)-Ph$_2$PZn$_2$-[(6,5) SWNT]** superstructures,[11,12g] to interrogate the optoelectronic properties of oxidized [(6,5) SWNTs]. Cyclic voltammetric experiments were used to directly determine the SWNT valence and conduction band energy levels in these assemblies; these studies demonstrate that SWNT potentiometric properties can be modulated by the nature of the electronic structure of the semiconducting polymer that wraps its surface and thereby define a new approach by which to regulate the magnitudes of SWNT exciton binding energies. Redox titration experiments establish electronic transitions uniquely associated with the SWNT hole polaron state and determine a hole polaron delocalization length of 2.75 nm for (6,5) SWNTs. Analysis of these electronic spectroscopic and potentiometric data acquired for oxidized (6,5) SWNTs within the context of a theoretical model developed by Spataru and Léonard[21c] and TD-DFT simulated transitions for a 4 nm-long bare $[(6,5)\ SWNT]^{2+}$ model structure strongly suggest that the experimental absorptions observed at ~1155 nm (Figure 2) and ~3400 cm^{-1} (Figure S14) for these polymer-[(6,5) SWNT] superstructures oxidized to achieve a hole densities of ~0.36 h/nm can be assigned to $E_{V2} \rightarrow E_{V1}$ and $E^{f}_{V_1} \rightarrow E^{V}_{V_1}$ transitions. Pump−probe TA spectroscopic data obtained for oxidized (6,5) SWNTs demonstrate: (i) a ground-state bleaching band centered at 1000 nm that is substantially broader than that determined for the analogous ground-state bleach observed for electronically excited neutral (6,5) SWNTs at equivalent time delays; (ii) that the prominent TA spectroscopic signals characteristic of the (6,5) SWNT hole polaron state are insensitive to the solvent dielectric environment; and (iii) faster ground-state bleach recovery dynamics consistent with SWNT hole polarons that are both delocalized and mobile. As these findings determine steady-state and transient electronic absorptive spectroscopic signatures that are uniquely associated with the (6,5) SWNT hole polaron state, this work enables more detailed characterization of charge-transfer reactions involving SWNTs and provides new insights for engineering the electronic structural properties of hybrid semiconducting polymer−nanotube assemblies.

ASSOCIATED CONTENT

Supporting Information

Experimental details, electrochemical data, electronic absorption spectra, redox titration data, Raman spectra, and TD-DFT data. This material is available free of charge via the Internet at http://pubs.acs.org.

AUTHOR INFORMATION

Corresponding Author

michael.therien@duke.edu

Notes

The authors declare no competing financial interest.

ACKNOWLEDGMENTS

This work was funded by the Division of Chemical Sciences, Geosciences, and Biosciences, Office of Basic Energy Sciences, of the U.S. Department of Energy through Grant DE-SC0001517. Infrastructural support was provided by the NSEC (DMR-0425780) program of the National Science Foundation.

REFERENCES

(1) (a) Bachilo, S. M.; Strano, M. S.; Kittrell, C.; Hauge, R. H.; Smalley, R. E.; Weisman, R. B. *Science* **2002**, *298*, 2361−2366. (b) O'Connell, M. J.; Bachilo, S. M.; Huffman, C. B.; Moore, V. C.; Strano, M. S.; Haroz, E. H.; Rialon, K. L.; Boul, P. J.; Noon, W. H.; Kittrell, C.; Ma, J.; Hauge, R. H.; Weisman, R. B.; Smalley, R. E. *Science* **2002**, *297*, 593−596. (c) Weisman, R. B.; Bachilo, S. M. *Nano Lett.* **2003**, *3*, 1235−1238.

(2) (a) Odom, T. W.; Huang, J.-L.; Kim, P.; Lieber, C. M. *Nature* **1998**, *391*, 62−64. (b) Wildöer, J. W. G.; Venema, L. C.; Rinzler, A. G.; Smalley, R. E.; Dekker, C. *Nature* **1998**, *391*, 59−62.

(3) Tans, S. J.; Devoret, M. H.; Dai, H.; Thess, A.; Smalley, R. E.; Geerligs, L. J.; Dekker, C. *Nature* **1997**, *386*, 474−477.
(4) (a) Guldi, D. M.; Rahman, G. M. A.; Prato, M.; Jux, N.; Qin, S.; Ford, W. *Angew. Chem., Int. Ed.* **2005**, *44*, 2015−2018. (b) Holt, J. M.; Ferguson, A. J.; Kopidakis, N.; Larsen, B. A.; Bult, J.; Rumbles, G.; Blackburn, J. L. *Nano Lett.* **2010**, *10*, 4627−4633.
(5) Tans, S. J.; Verschueren, A. R. M.; Dekker, C. *Nature* **1998**, *393*, 49−52.
(6) Aguirre, C. M.; Auvray, S.; Pigeon, S.; Izquierdo, R.; Desjardins, P.; Martel, R. *Appl. Phys. Lett.* **2006**, *88*, 183104.
(7) Barone, P. W.; Baik, S.; Heller, D. A.; Strano, M. S. *Nat. Mater.* **2005**, *4*, 86−92.
(8) (a) Paolucci, D.; Franco, M. M.; Iurlo, M.; Marcaccio, M.; Prato, M.; Zerbetto, F.; Pénicaud, A.; Paolucci, F. *J. Am. Chem. Soc.* **2008**, *130*, 7393−7399. (b) Zheng, M.; Diner, B. A. *J. Am. Chem. Soc.* **2004**, *126*, 15490−15494. (c) O'Connell, M. J.; Eibergen, E. E.; Doorn, S. K. *Nat. Mater.* **2005**, *4*, 412−418.
(9) (a) McDonald, T. J.; Svedruzic, D.; Kim, Y.-H.; Blackburn, J. L.; Zhang, S. B.; King, P. W.; Heben, M. J. *Nano Lett.* **2007**, *7*, 3528−3534. (b) Tanaka, Y.; Hirana, Y.; Niidome, Y.; Kato, K.; Saito, S.; Nakashima, N. *Angew. Chem., Int. Ed.* **2009**, *48*, 7655−7659.
(10) (a) Aitola, K.; Kaskela, A.; Halme, J.; Ruiz, V.; Nasibulin, A. G.; Kauppinen, E. I.; Lund, P. D. *J. Electrochem. Soc.* **2010**, *157*, B1831−B1837. (b) Rosario-Canales, M. R.; Deria, P.; Therien, M. J.; Santiago-Avilés, J. J. *ACS Appl. Mater. Interfaces* **2012**, *4*, 102−109.
(11) Deria, P.; Von Bargen, C. D.; Olivier, J.-H.; Kumbhar, A. S.; Saven, J. G.; Therien, M. J. *J. Am. Chem. Soc.* **2013**, *135*, 16220−16234.
(12) (a) Kang, Y. K.; Lee, O.-S.; Deria, P.; Kim, S. H.; Park, T.-H.; Bonnell, D. A.; Saven, J. G.; Therien, M. J. *Nano Lett.* **2009**, *9*, 1414−1418. (b) Deria, P.; Sinks, L. E.; Park, T.-H.; Tomezsko, D. M.; Brukman, M. J.; Bonnell, D. A.; Therien, M. J. *Nano Lett.* **2010**, *10*, 4192−4199. (c) Park, J.; Deria, P.; Therien, M. J. *J. Am. Chem. Soc.* **2011**, *133*, 17156−17159. (d) Larsen, B. A.; Deria, P.; Holt, J. M.; Stanton, I. N.; Heben, M. J.; Therien, M. J.; Blackburn, J. L. *J. Am. Chem. Soc.* **2012**, *134*, 12485−12491. (e) Bonhommeau, S.; Deria, P.; Glesner, M. G.; Talaga, D.; Najjar, S.; Belin, C.; Auneau, L.; Trainini, S.; Therien, M. J.; Rodriguez, V. *J. Phys. Chem. C* **2013**, *117*, 14840−14849. (f) Von Bargen, C. D.; MacDermaid, C. M.; Lee, O.-S.; Deria, P.; Therien, M. J.; Saven, J. G. *J. Phys. Chem. B* **2013**, *117*, 12953−12965. (g) Olivier, J.-H.; Deria, P.; Park, J.; Kumbhar, A.; Andrian-Albescu, M.; Therien, M. J. *Angew. Chem., Int. Ed.* **2013**, *52*, 13080−13085. (h) Park, J.; Deria, P.; Olivier, J.-H.; Therien, M. J. *Nano Lett.* **2014**, *14*, 504−511.
(13) (a) Arnold, M. S.; Green, A. A.; Hulvat, J. F.; Stupp, S. I.; Hersam, M. C. *Nat. Nanotechnol.* **2006**, *1*, 60−65. (b) Ghosh, S.; Bachilo, S. M.; Weisman, R. B. *Nat. Nanotechnol.* **2010**, *5*, 443−450.
(14) Frisch, M. J.; Trucks, G. W.; Schlegel, H. B.; Scuseria, G. E.; Robb, M. A.; Cheeseman, J. R.; Scalmani, G.; Barone, V.; Mennucci, B.; Petersson, G. A.; Nakatsuji, H.; Caricato, M.; Li, X.; Hratchian, H. P.; Izmaylov, A. F.; Bloino, J.; Zheng, G.; Sonnenberg, J. L.; Hada, M.; Ehara, M.; Toyota, K.; Fukuda, R.; Hasegawa, J.; Ishida, M.; Nakajima, T.; Honda, Y.; Kitao, O.; Nakai, H.; Vreven, T.; Montgomery, J. A., Jr.; Peralta, J. E.; Ogliaro, F.; Bearpark, M.; Heyd, J. J.; Brothers, E.; Kudin, K. N.; Staroverov, V. N.; Kobayashi, R.; Normand, J.; Raghavachari, K.; Rendell, A.; Burant, J. C.; Iyengar, S. S.; Tomasi, J.; Cossi, M.; Rega, N.; Millam, J. M.; Klene, M.; Knox, J. E.; Cross, J. B.; Bakken, V.; Adamo, C.; Jaramillo, J.; Gomperts, R.; Stratmann, R. E.; Yazyev, O.; Austin, A. J.; Cammi, R.; Pomelli, C.; Ochterski, J. W.; Martin, R. L.; Morokuma, K.; Zakrzewski, V. G.; Voth, G. A.; Salvador, P.; Dannenberg, J. J.; Dapprich, S.; Daniels, A. D.; Farkas, Ö.; Foresman, J. B.; Ortiz, J. V.; Cioslowski, J.; Fox, D. J. *Gaussian 09*, revision A.1; Gaussian Inc.: Wallingford, CT, 2009.
(15) Tretiak, S. *Nano Lett.* **2007**, *7*, 2201−2206.
(16) (a) Kleinhenz, N.; Yang, L.; Zhou, H.; Price, S. C.; You, W. *Macromolecules* **2011**, *44*, 872−877. (b) You, W.; Wang, L.; Wang, Q.; Yu, L. *Macromolecules* **2002**, *35*, 4636−4645. (c) Cardona, C. M.; Li, W.; Kaifer, A. E.; Stockdale, D.; Bazan, G. C. *Adv. Mater.* **2011**, *23*, 2367−2371.
(17) Dean, J. A.; Lange, N. A. *Lange's Handbook of Chemistry*, 15th ed.; McGraw-Hill: New York, 1999.
(18) Campbell, J. F.; Napier, M. E.; Feldberg, S. W.; Thorp, H. H. *J. Phys. Chem. B* **2010**, *114*, 8861−8870.
(19) Shabangi, M.; Kuhlman, M. L.; Flowers, R. A., II *Org. Lett.* **1999**, *1*, 2133.
(20) (a) Ma, Y.-Z.; Valkunas, L.; Bachilo, S. M.; Fleming, G. R. *J. Phys. Chem. B* **2005**, *109*, 15671−15674. (b) Wang, F.; Dukovic, G.; Brus, L. E.; Heinz, T. *Science* **2005**, *308*, 838−841. (c) Dukovic, G.; Wang, F.; Song, D. H.; Sfeir, M. Y.; Heinz, T. F.; Brus, L. E. *Nano Lett.* **2005**, *5*, 2314−2318.
(21) (a) Matsunaga, R.; Matsuda, K.; Kanemitsu, Y. *Phys. Rev. Lett.* **2011**, *106*, 037404. (b) Mouri, S.; Matsuda, K. *J. Appl. Phys.* **2012**, *111*, 094309. (c) Spataru, C. D.; Léonard, F. *Phys. Rev. Lett.* **2010**, *104*, 177402.
(22) Lüer, L.; Hoseinkhani, S.; Polli, D.; Crochet, J.; Hertel, T.; Lanzani, G. *Nat. Phys.* **2009**, *5*, 54−58.
(23) (a) Zhou, W.; Vavro, J.; Nemes, N. M.; Fischer, J. E.; Borondics, F.; Kamarás, K.; Tanner, D. B. *Phys. Rev. B* **2005**, *71*, 205423. (b) Blackburn, J. L.; Barnes, T. M.; Beard, M. C.; Kim, Y.-H.; Tenent, R. C.; McDonald, T. J.; To, B.; Coutts, T. J.; Heben, M. J. *ACS Nano* **2008**, *2*, 1266−1274.
(24) (a) Rønnow, T. F.; Pedersen, T. G.; Cornean, H. D. *Phys. Rev. B* **2010**, *81*, 205446. (b) Niklas, J.; Holt, J. M.; Mistry, K.; Rumbles, G.; Blackburn, J. L.; Poluektov, O. G. *J. Phys. Chem. Lett.* **2014**, *5*, 601−606.
(25) Saito, R.; Dresselhaus, G.; Dresselhaus, M. S. *Physical Properties of Carbon Nanotubes*; Imperial College Press: London, 1998.
(26) Itkis, M. E.; Niyogi, S.; Meng, M. E.; Hamon, M. A.; Hu, H.; Haddon, R. C. *Nano Lett.* **2002**, *2*, 155−159.
(27) Note, for example, that this shift is of larger magnitude for the ***S*-PBN(b)-Ph$_4$PhCN** polymer relative to that effected by the ***S*-PBN(b)-Ph$_5$** polymer.
(28) Miyauchi, Y.; Oba, M.; Maruyama, S. *Phys. Rev. B* **2006**, *74*, 205440.
(29) Zhou, Z.; Steigerwald, M.; Hybertsen, M.; Brus, L.; Friesner, R. A. *J. Am. Chem. Soc.* **2004**, *126*, 3597−3607.
(30) Rochefort, A.; Salahub, D. R.; Avouris, P. *J. Phys. Chem. B* **1999**, *103*, 641−646.
(31) Dukovic, G.; White, B. E.; Zhou, Z.; Wang, F.; Jockusch, S.; Steigerwald, M. L.; Heinz, T. F.; Friesner, R. A.; Turro, N. J.; Brus, L. E. *J. Am. Chem. Soc.* **2004**, *126*, 15269−15276.
(32) (a) Crochet, J. J.; Duque, J. G.; Werner, J. H.; Doorn, S. K. *Nat. Nanotechnol.* **2012**, *7*, 126−132. (b) Nishihara, T.; Yamada, Y.; Kanemitsu, Y. *Phys. Rev. B* **2012**, *86*, 075449. (c) Nishihara, T.; Yamada, Y.; Okano, M.; Kanemitsu, Y. *Appl. Phys. Lett.* **2013**, *103*, 023101.